Supporting Information

Pr_6O_{11}-driven electron modulation via d-f orbital hybridization for alkaline seawater electrolysis

Nana Chen,[a,b] Bari Wulan,[b]* Weipeng Zhang,[b] Xinping Xie,[b] Yuying Zhao,[b] Haibin Guan,[b] Dongxing Tan,[c] Lei Chen,[b] Baofeng Zhao,[b] Weihong Zhou[a]*

[a] *School of Civil Engineering, University of Science and Technology Liaoning, Anshan 114051 China*

[b] *Energy Research Institute, Shandong Key Laboratory of Biomass Efficient Conversion and Utilization, Qilu University of Technology (Shandong Academy of Sciences), Jinan 250014 China*

[c] *Shandong Key Laboratory of Catalytic Conversion and Clean Energy, School of Chemistry and Chemical Engineering, Qufu Normal University, Qufu 273165 China*

*Corresponding authors: bariwulan@qlu.edu.cn (B. Wulan), zwh_0190@sina.cn (W. Zhou)

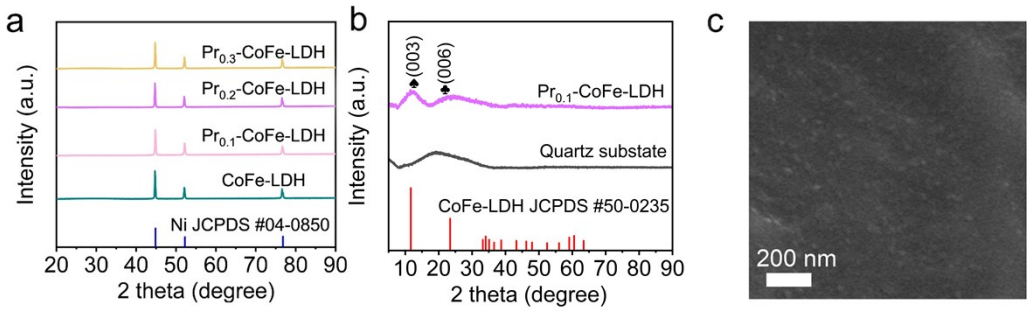

Fig. S1. XRD patterns of Pr_x-CoFe-LDH deposited on the surface of (a) nickel mesh and (b) blank quartz. (c) SEM image of CoFe-LDH deposited on the surface of Ni mesh.

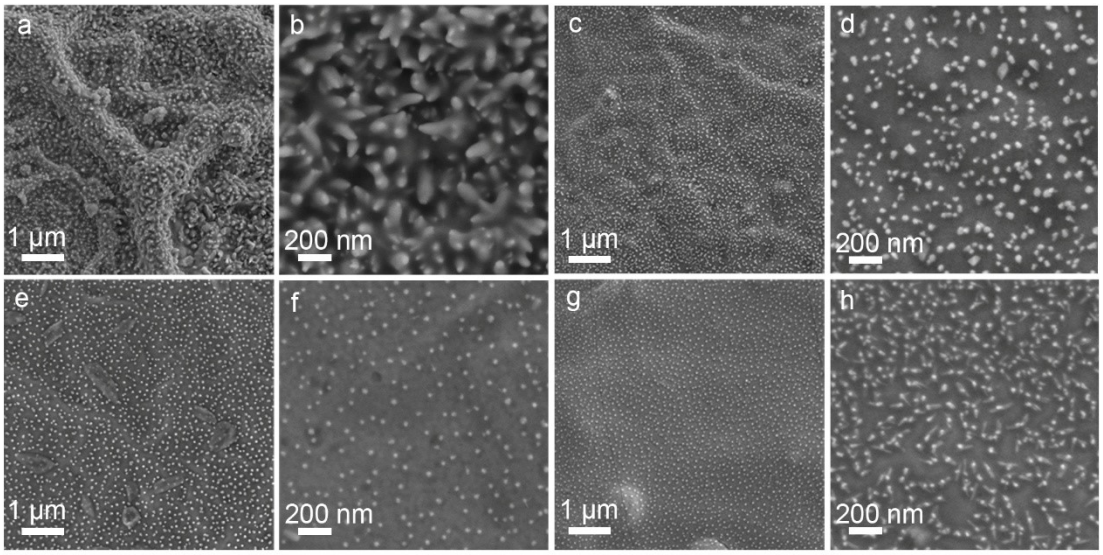

Fig. S2. SEM images of (a, b) CoP/Fe_2P, (c, d) $Pr_{0.1}$-CoP/Fe_2P, (e, f) $Pr_{0.2}$-CoP/Fe_2P, and (g, h) $Pr_{0.3}$-CoP/Fe_2P.

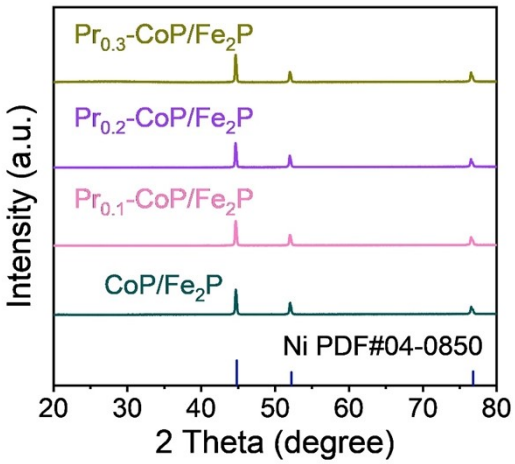

Fig. S3. XRD patterns of the as-prepared Pr_x-CoFe-LDH electrodes after the phosphidation treatment.

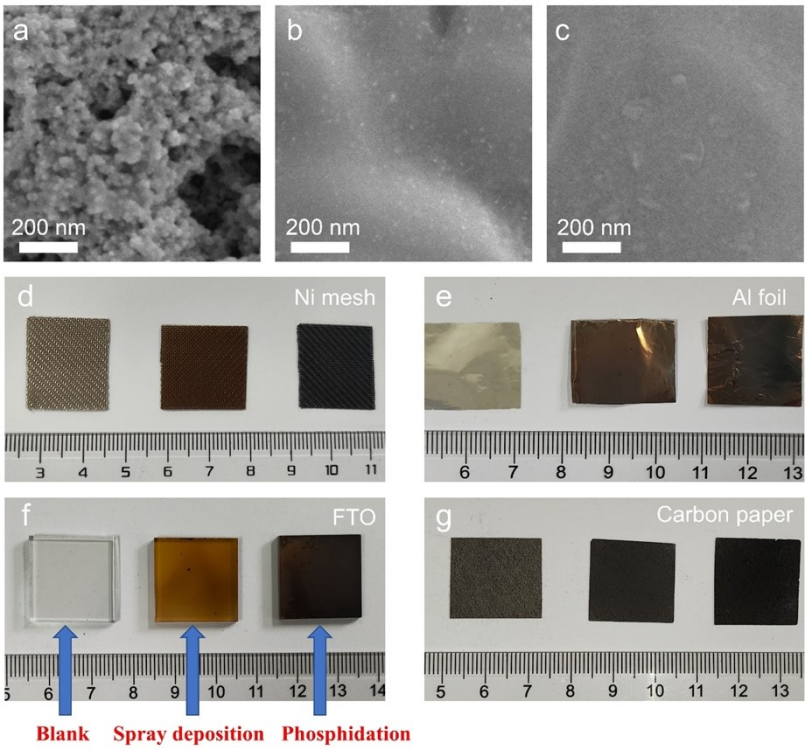

Fig. S4. SEM images of spray-deposited CoFe-LDH on (a) carbon paper, (b) Al foil, and (c) FTO. (d-g) Photographs of Pr_x-CoP/Fe_2P grown on different substrates via spray deposition followed by phosphidation.

Specifically, uniformly distributed nanoparticles are observed on carbon paper after identical spray deposition, whereas dense and uniform coatings are formed on Al foil and FTO. The substrate-dependent morphologies differ from those on Ni mesh, which may be attributed to different interactions between the metal salt species and the substrate during spray deposition, leading to distinct nucleation and growth behaviors.

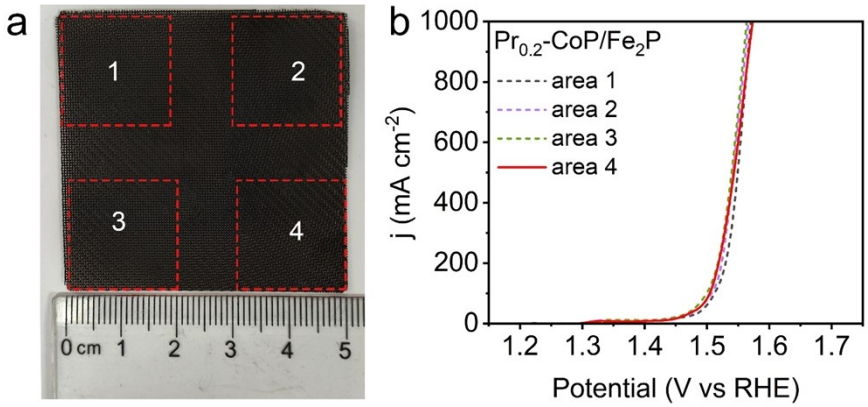

Fig. S5. (a) Photograph of the as-prepared $Pr_{0.2}$-CoP/Fe_2P electrode (5 × 5 cm^2). (b) Polarization curves collected from selected regions of the electrode.

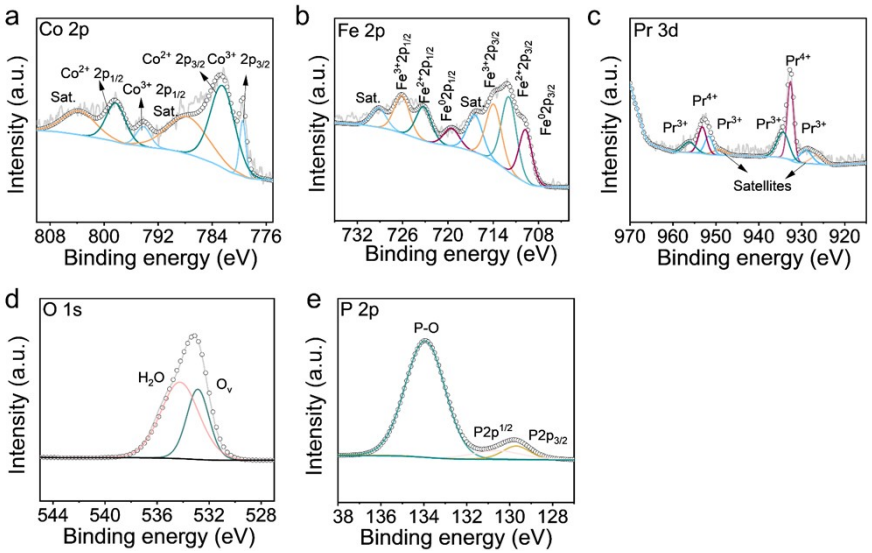

Fig. S6. High-resolution XPS spectra of (a) Co 2p, (b) Fe 2p, (c) Pr 3d, (d) O 1s, and (e) P 2p at $Pr_{0.1}$-CoP/Fe_2P electrode.

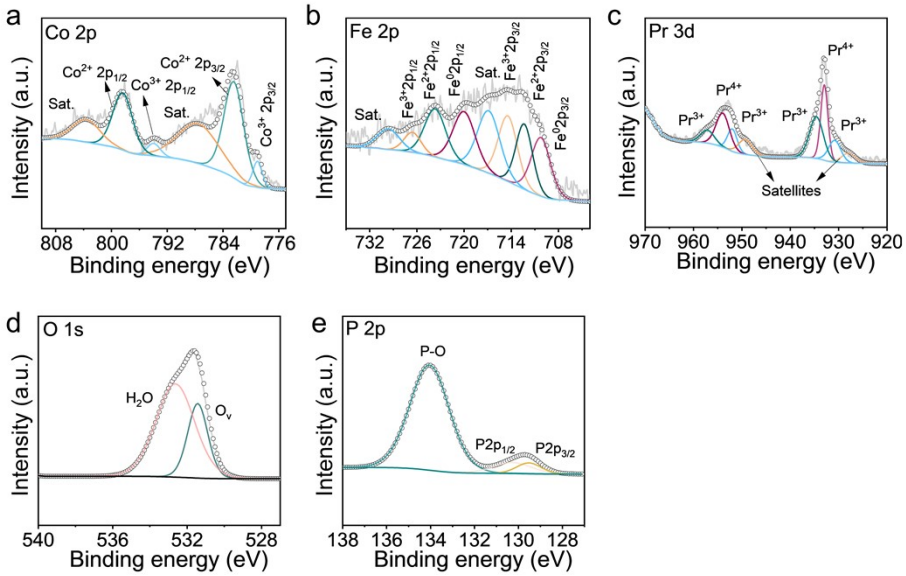

Fig. S7. High-resolution XPS spectra of (a) Co 2p, (b) Fe 2p, (c) Pr 3d, (d) O 1s, and (e) P 2p at $Pr_{0.3}$-CoP/Fe_2P electrode.

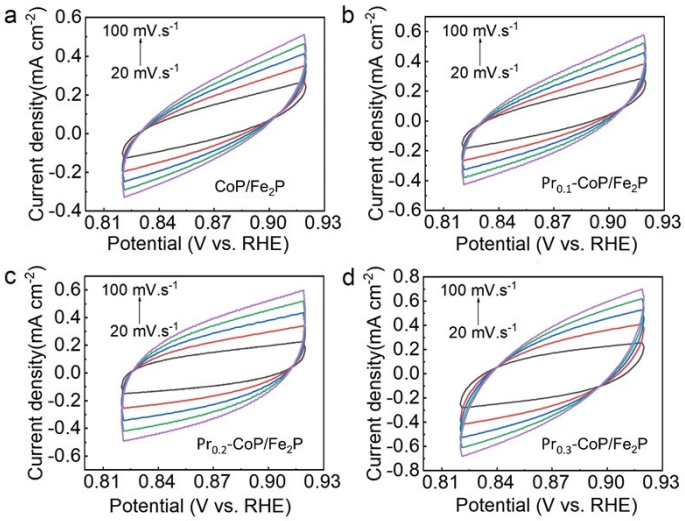

Fig. S8. CV curves for (a) CoP/Fe_2P, (b) $Pr_{0.1}$-CoP/Fe_2P, (c) $Pr_{0.2}$-CoP/Fe_2P and (d) $Pr_{0.3}$-CoP/Fe_2P.

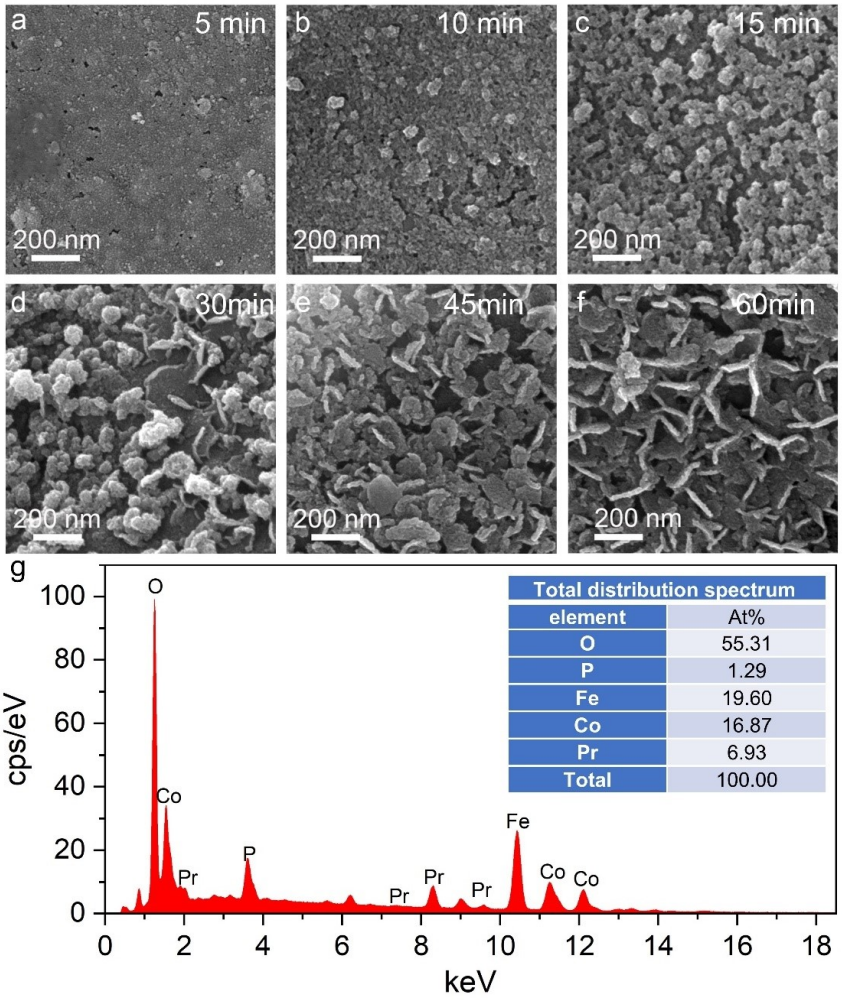

Fig. S9. SEM images of $Pr_{0.2}$-CoP/Fe_2P during OER process at 200 mA cm^{-2} for (a) 5 min, (b) 10 min, (c) 15 min, (d) 30 min, (e) 45 min, and (f) 60 min. (g) The EDS spectrum of $Pr_{0.2}$-Co_2P/FeP after OER.

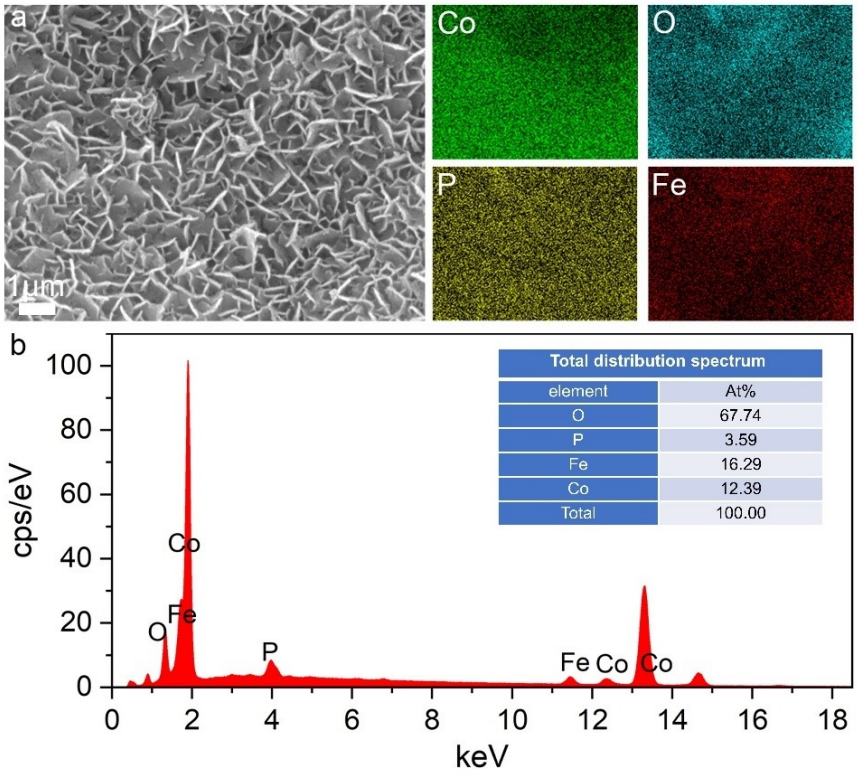

Fig. S10. (a) SEM image and (b) the corresponding EDS spectrum of CoP/Fe_2P after OER test.

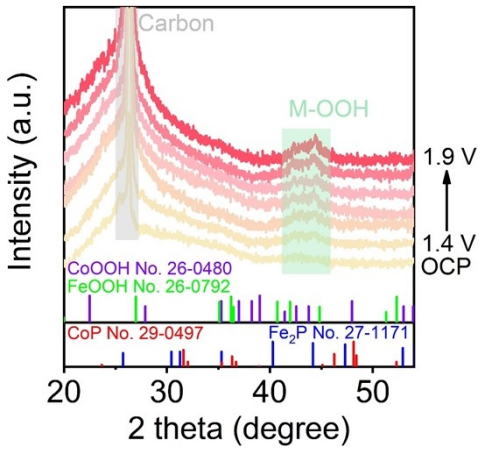

Fig. S11. Semi in situ XRD patterns of $Pr_{0.2}$-CoP/Fe_2P during the OER process.

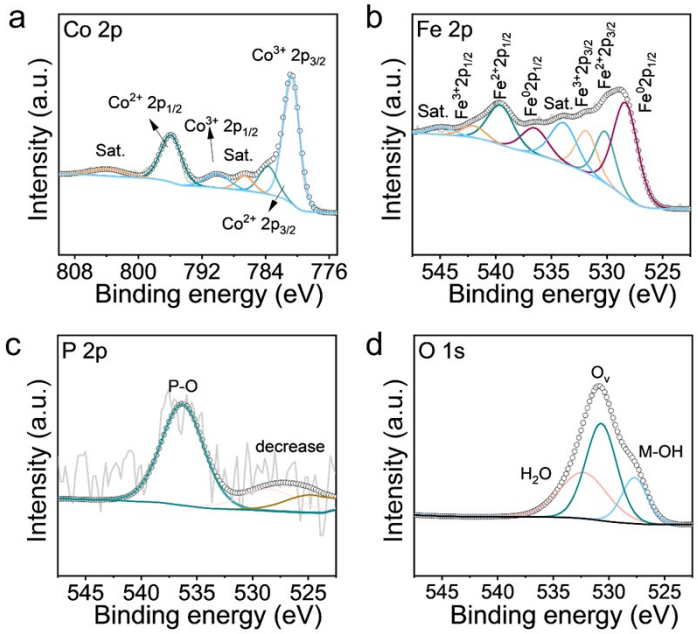

Fig. S12. High-resolution (a) Co 2p, (b) Fe 2p, (c) P 2p, and (d) O 1s XPS spectra of CoP/Fe_2P after OER.

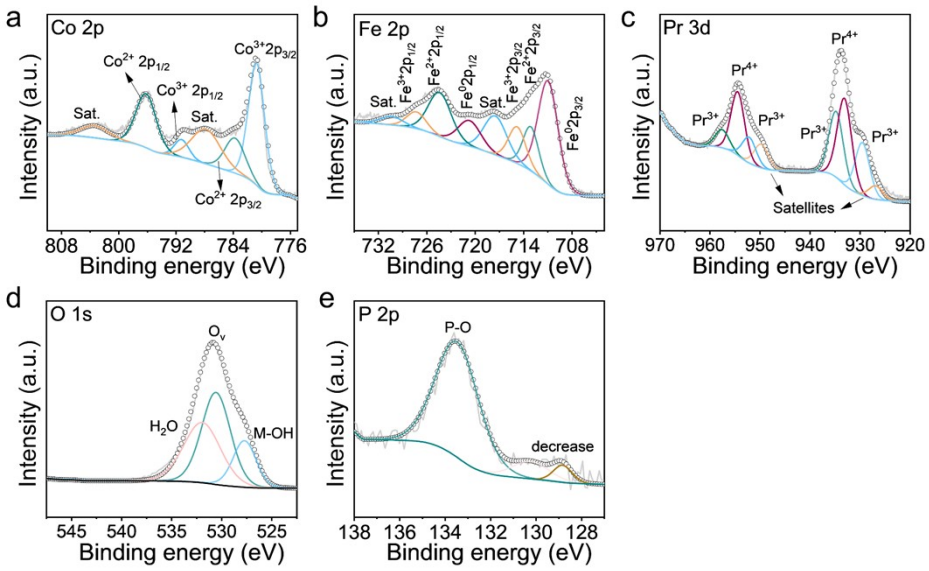

Fig. S13. High-resolution (a) Co 2p, (b) Fe 2p, (c) Pr 3d, (d) O 1s, and (e) P 2p XPS spectra of $Pr_{0.1}$-CoP/Fe_2P after OER.

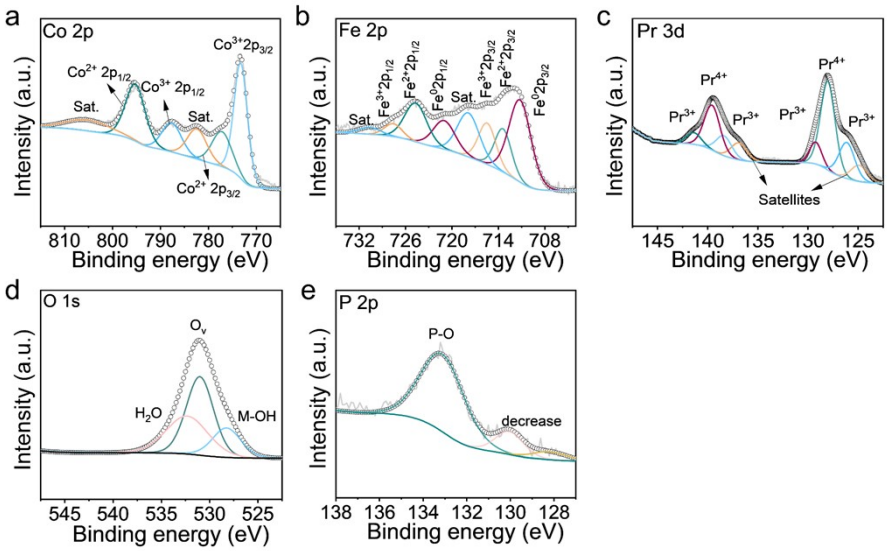

Fig. S14. High-resolution (a) Co 2p, (b) Fe 2p, (c) Pr 3d, (d) O 1s, and (e) P 2p XPS spectra of $Pr_{0.3}$-CoP/Fe_2P after OER.

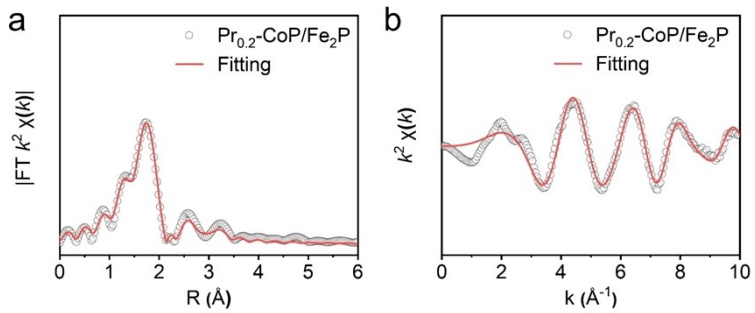

Fig. S15. The Fe K-edge EXAFS (a) R space and (b) k space fitting curves for $Pr_{0.2}$-CoP/Fe_2P after OER.

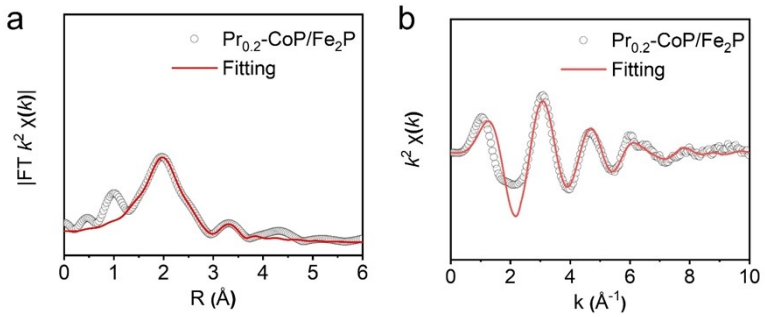

Fig. S16. The Pr L_3-edge EXAFS (a) R space and (b) k space fitting curves for $Pr_{0.2}$-CoP/Fe_2P after OER.

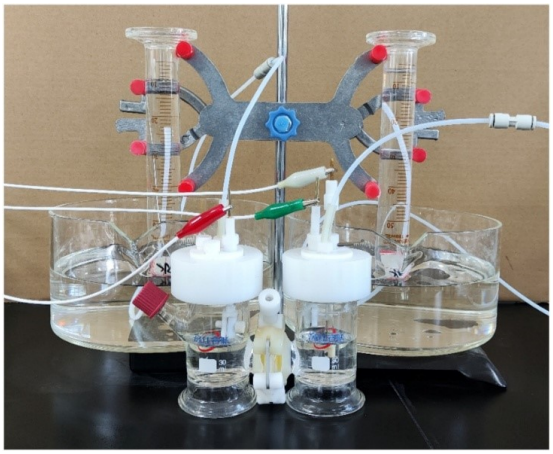

Fig. S17. Photograph of the apparatus for testing gas volumes generated by a drainage method.

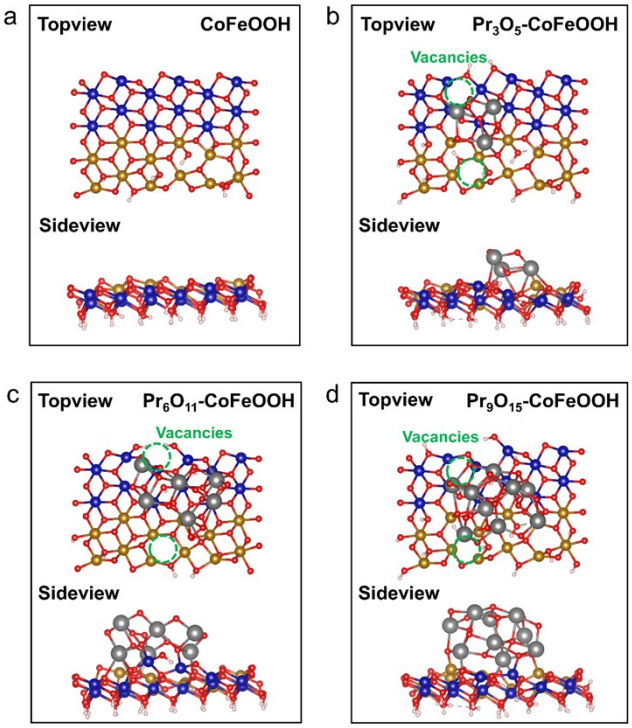

Fig. S18. The optimized structure of (a) CoFeOOH, (b) Pr_3O_5-CoFeOOH, (c) Pr_6O_{11}-CoFeOOH, and (d) Pr_9O_{15}-CoFeOOH.

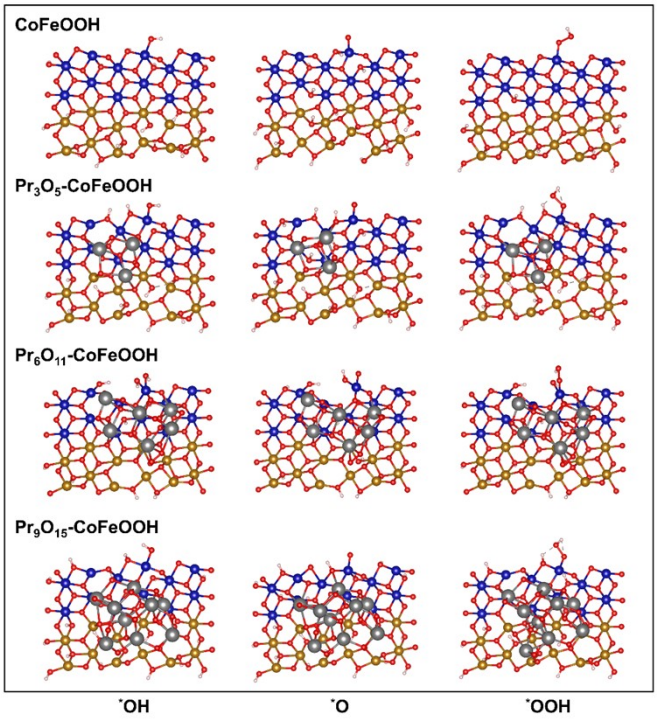

Fig. S19. The optimized OER configuration of reaction intermediates on different structures.

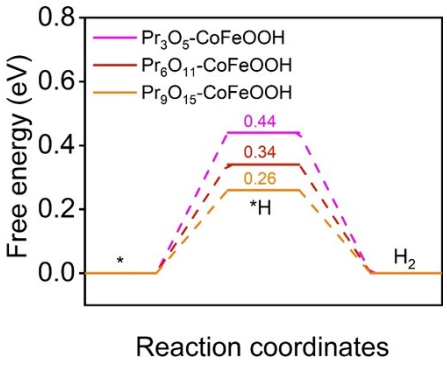

Fig. S20. Calculated Gibbs free energy profiles for the HER on different structures.

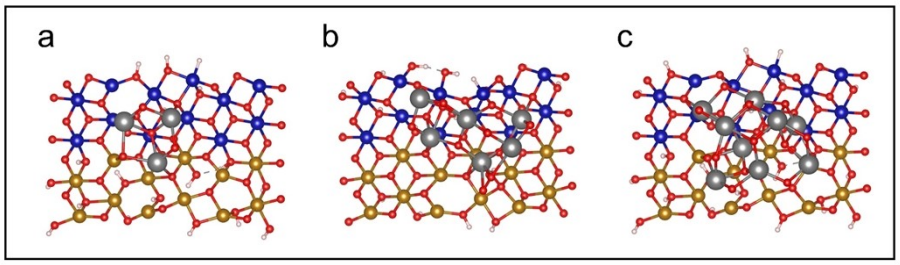

Fig. S21. The optimized configuration of *H on (a) Pr_3O_5-CoFeOOH, (b) Pr_6O_{11}-CoFeOOH, and (c) Pr_9O_{15}-CoFeOOH.

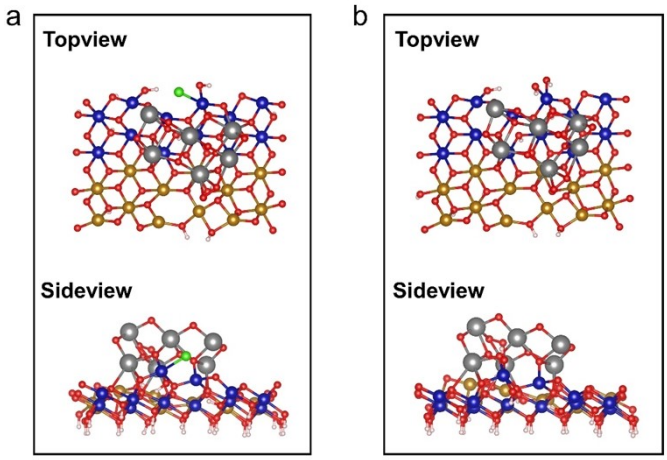

Fig. S22. The optimized configuration of (a) Cl^- and (b) OH^- adsorbed on the surface of Pr_6O_{11}-CoFeOOH.

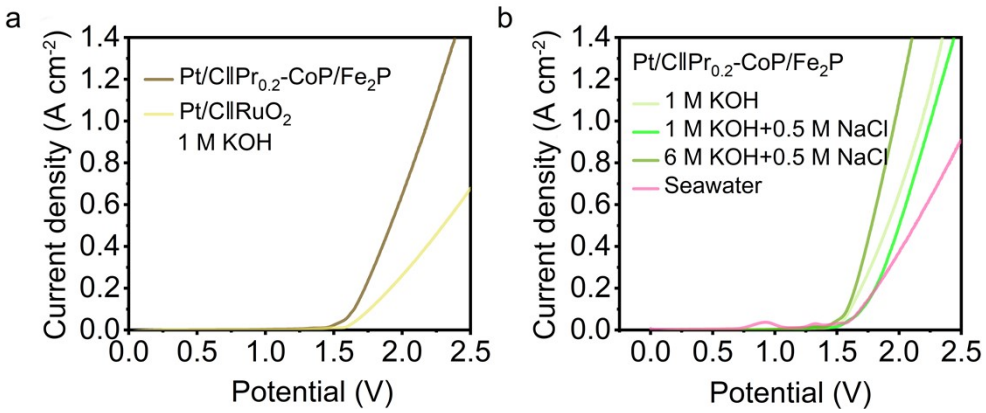

Fig. S23. (a) Polarization curves of AEMWE with different catalysts in 1 M KOH at room temperature. (b) Polarization curves of AEMWE using $Pr_{0.2}$-CoP/Fe_2P as the anode and Pt/C as the cathode in different electrolytes at 60°C.

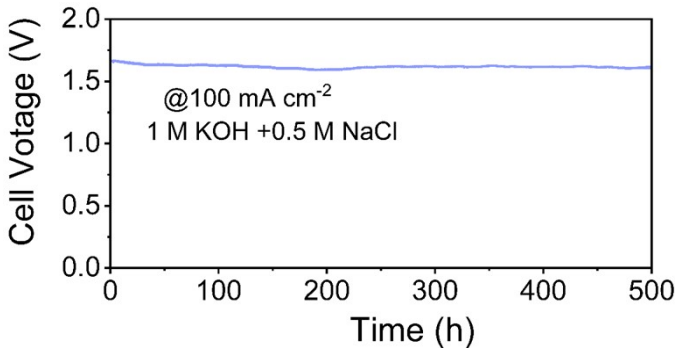

Fig. S24. Stability test of AEMWE with Pt/C || $Pr_{0.2}$-CoP/Fe_2P in 1 M KOH + 0.5 M NaCl at room temperature.

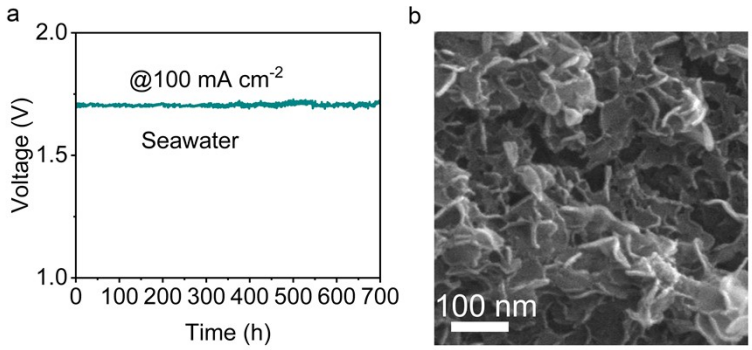

Fig. S25. (a) Chronopotentiometric durability of $Pr_{0.2}$-CoP/Fe_2P in natural seawater over 300 h. (b) SEM image of $Pr_{0.2}$-CoP/Fe_2P after stability test.

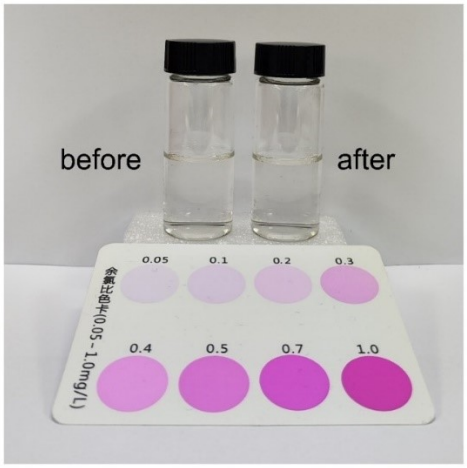

Fig. S26. Result of colorimetric reagent testing for the presence of hypochlorite in the 1 M KOH + 0.5 M NaCl electrolyte after stability testing of $Pr_{0.2}$-CoP/Fe_2P electrode at 100 mA cm^{-2} for 500 h.

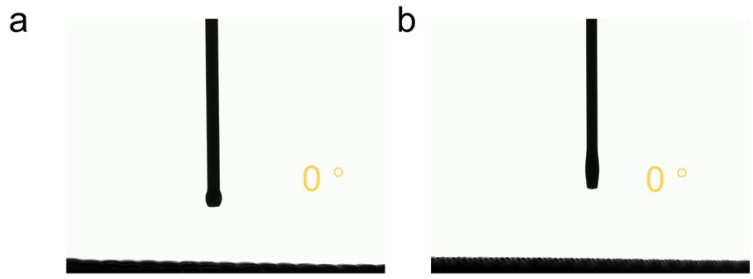

Fig. S27. Static water contact angle of (a) CoP/Fe_2P and (b) $Pr_{0.2}$-CoP/Fe_2P electrode in 1 M KOH.

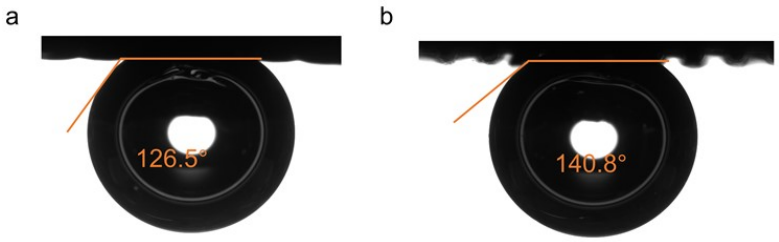

Fig. S28. Bubble contact angles in 1 M KOH for (a) CoP/Fe_2P and (b) $Pr_{0.2}$-CoP/Fe_2P.

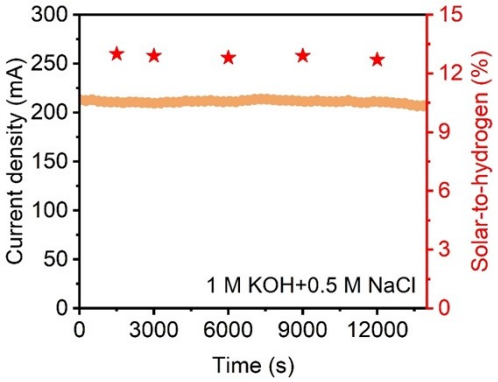

Fig. S29 Photovoltaic-driven stability test and the corresponding STH conversion efficiency.

Table S1. Overpotential comparison of recently reported non-noble-metal OER electrocatalysts.

Samples	Overpotential (mV, at 100 mA cm^{-2})	Electrolyte	Ref.
$Pr_{0.2}$-CoP/Fe_2P	223	1 M KOH	This work
$NiCe_{0.05}$/Fe@NM	257	1 M KOH	[1]
MIM@Fe0.10-CoNi CH/NF	~270	1 M KOH	[2]
NiFe-LDH/FF	220	1 M KOH	[3]
F,Fe-CoO	~230	1 M KOH	[4]
R-CoFe/Ce/NF	~299	1 M KOH	[5]
Mo-Ni_2P/Fe_xP-V/NFF	246	1 M KOH	[6]
Mo-Co_9S_8@CC-2	279	1 M KOH	[7]
NiFe-LDH/Ni_2S_2	~245	1 M KOH	[8]
S-NiFeZn LDH/NF	235	1 M KOH	[9]
P-$NiCuFe_{0.06}$-LDH	240	1 M KOH	[10]
$Fe_{2.5}Co_{2.5}Ni_{10}$OyHz@NFF	229	1 M KOH	[11]
Mo-FeNiP NTs/NF	232.6	1 M KOH	[12]
D/CoFc-MOF	~275	1 M KOH	[13]
NiFe-LS	~215	1 M KOH	[14]
S-FeOOH/$Co(OH)_2$/NF	252	1 M KOH	[15]
NiFeMo IOS @ NF	~225	1 M KOH	[16]
Ru-SAC/NiFe LDH	~218	1 M KOH	[17]
CFP	296	1 M KOH	[18]
Se/Fe-CoP AGs	297	1 M KOH	[19]
Ru-S-NiFe LDH	~275	1 M KOH	[20]
VFe-$Ni_{12}P_5$@C	251	1 M KOH	[21]

Table S2. Comparison of recently reported rare-earth-modified transition-metal (oxy)hydroxide catalysts for OER.

Catalyst	Tafel slope ($mV\ dec^{-1}$)	Electrolyte	Overpotential (mV)	Stability (h)	Ref.
$Pr_{0.1}$-CoP/Fe_2P	46.9	1M KOH	223 at 100 mA cm^{-2}	500 h	This work
LaFeCoOOH	44.1	1M KOH	177 at 10 mA cm^{-2}	1000 h	[22]
$NiSe_2$-$Ce_2(CO_3)_2O$	86.2	1M KOH	268 at 50 mA cm^{-2}	120 h	[23]
Er droped CoP	70	1M KOH	256 at 10 mA cm^{-2}	20 h	[24]
NdNi-Co_3O_4	54	1M KOH	269 at 10 mA cm^{-2}	50 h	[25]
Eu_2O_3/Fe_3O_4@NCG-900	68.3	1M KOH	269 at 10 mA cm^{-2}	1000 h	[26]
$Er_{0.4}$Fe-MOF/NF	73	1M KOH	248 at 100 mA cm^{-2}	100 h	[27]
Co/CeO_2-NCNA@CC	98	1M KOH	350 at 10 mA cm^{-2}	380 h	[28]
FeCoNiMoCeHEA/C	63.4	1M KOH	260 at 10 mA cm^{-2}	/	[29]
CeO_2/Ni_3FeN/Ni_3Fe-5%NPs	52.7	1M KOH	249 at 10 mA cm^{-2}	24 h	[10]
La-CoMoP	86.5	1M KOH	250 at 10 mA cm^{-2}	24 h	[30]

Table S3. Quantitative XPS valence-state distributions of Fe, Co, and Pr before and after reaction

Sample	Co species (%)		Fe species (%)		Pr species (%)	
	Co^{2+}	Co^{3+}	Fe^{2+}	Fe^{3+}	Pr^{3+}	Pr^{4+}
CoP/Fe_2P	40.17	28.34	20.25	46.77	/	/
$Pr_{0.1}$-CoP/Fe_2P	37.58	25.01	33.45	29.48	40.52	49.04
$Pr_{0.2}$-CoP/Fe_2P	43.50	28.86	39.58	34.30	45.87	40.2
$Pr_{0.3}$-CoP/Fe_2P	38.99	21.86	26.68	20.16	33.23	57.62
CoP/Fe_2P-OER	32.93	57.33	15.51	27.49	/	/
$Pr_{0.1}$-CoP/Fe_2P-OER	32.34	51.51	15.02	26.10	35.15	53.98
$Pr_{0.2}$-CoP/Fe_2P-OER	33.17	51.06	18.13	33.26	36.26	45.81
$Pr_{0.3}$-CoP/Fe_2P-OER	32.41	50.77	15.53	22.19	41.90	45.36

Table S4. EXAFS fitting results for Pr foil, Fe foil, FeO, Fe_2O_3, and $Pr_{0.2}$-CoP/Fe_2P after OER at the Fe K-edge and Pr L_3-edge.

Sample	Shell	Bond length (Å)	Coordination Number	σ^2 (Å^2)	E0 shift (eV)	R-factor
Fe foil	Fe-Fe	2.46±0.02	8*	0.005±0.002	-2.4±3.7	0.009
	Fe-Fe	2.85±0.02	6*	0.005±0.004		
FeO	Fe-O	2.13±0.01	6*	0.016±0.002	-1.8±0.8	0.009
	Fe-Fe	3.08±0.01	12*	0.014±0.001		
Fe_2O_3	Fe-O	1.98±0.02	6*	0.009±0.003	-4.8±1.7	0.015
	Fe-Fe	2.92±0.02	3*	0.003±0.002		
	Fe-Fe	3.36±0.03	3*	0.005±0.002		
	Fe-O	3.47±0.04	3*	0.013±0.003		
	Fe-O	3.61±0.04	3*	0.010±0.005		
Pr foil	Pr-Pr	3.32±0.01	8*	0.011±0.002	-5.6±3.1	0.019
	Pr-Pr	3.81±0.02	6*	0.013±0.002		
sample	Fe-O	1.98±0.04	5.4±0.3	0.014±0.004	-2.1±2.4	0.020
	Fe-Fe	3.02±0.02	2.2±0.4	0.015±0.004		
	Fe-Fe	3.48±0.03	3.7±0.5	0.008±0.006		
	Pr-O	2.43±0.01	4.8±0.7	0.012±0.003	-6.5±0.9	0.018
	Pr-O	2.61±0.04	3.3±1.0	0.014±0.002		
	Pr-Pr	3.94±0.02	3.7±0.9	0.009±0.004		

Table S5. ICP results of $Pr_{0.2}$-CoP/Fe_2P after OER.

Elements	Molar mass (μmol)
Fe	3.83
Co	3.87
Pr	1.95

Table S6. Comparison of the water-splitting performance of our AEMWE with other recently reported water electrolyzer.

Catalyst	Performance	Conditions	Stability	Ref.
Pt/C||$Pr_{0.2}$-CoP/Fe_2P	1.88 V@1 A cm^{-2}	85°C, 30 wt% KOH	400 h @300 mA cm^{-2} (1 M KOH at 25°C)	This work
FeRu@NM-2||FeRu@NM-2	2.19 V@1 A cm^{-2}	60°C, 1 M KOH	90 h @500 mA cm^{-2} (1 M KOH at 60°C)	31
CuNi@NiSe||CuNi@NiSe	2.2 V@1 A cm^{-2}	80°C, 1 M KOH	10 h @1000 mA cm^{-2} (1 M KOH at 80°C)	32
Ru-Co_2NiNCNT||Ru-Co_2NiNCNT	1.87 V@1 A cm^{-2}	60°C, 1 M KOH	400 h @500 mA cm^{-2} (1 M KOH at 60°C)	33
$Co_{2.8}W_{3.8}$-NiFe LDH||Pt/C	1.86 V@1 A cm^{-2}	60°C, 1 M KOH	300 h @1000 mA cm^{-2} (1 M KOH at 60°C)	34
$NiCe_{0.05}$/Fe@NM|| $NiCe_{0.05}$/Fe@NM	2.27 V@1 A cm^{-2}	60°C, 5 M KOH	70 h @1000 mA cm^{-2} (5 M KOH at 60°C)	1
$Ni_3FeN@PO_4^{3-}$/NF||Pt-Ni@MoN/NF	2.11 V@1A cm^{-2}	25°C 6 M KOH + seawater	140 h @1000 mA cm^{-2} (6 M KOH + seawater at 25°C)	35

Table S7. ICP analysis of dissolved Fe, Co, and Pr in the electrolyte after 300 h OER testing.

Sample	Fe (mg/L)	Co (mg/L)	Pr (mg/L)
$Pr_{0.2}$-CoP/Fe_2P	0.09	0.04	0.06

Reference:

1 W. Yaseen, M. Xie, B. A. Yusuf, S. C. Meng, I. Khan, J. M. Xie and Y. G. Xu, Small, 2024, **20**, 2403971.

2 H. W. Tang, Z. Y. Sun, S. Y. Fan, S. W. Feng, L. Li, L. Fang and C. J. Wang, Chem. Eng. J., 2024, **491**, 152023.

3 J. W. Li, M. Song, Y. Z. Hu, C. Zhang, W. Liu, X. Huang, J. J. Zhang, Y. Zhu, J. Zhang and D. L. Wang, Nano Res., 2023, **16**, 3658-3664.

4 P. C. Ye, K. Q. Fang, H. Y. Wang, Y. H. Wang, H. Huang, C. B. Mo, J. Q. Ning and Y. Hu, Nat. Commun., 2024, **15**, 1012.

5 Y. Deng, J. Wang, S. F. Zhang, Z. J. Zhang, J. F. Sun, T. T. Li, J. L. Kang, H. Liu and S. Bai, Rare Met., 2025, **44**, 1053-1066.

6 X. H. Xu, K. W. Guo, J. K. Sun, X. Y. Yu, X. Y. Miao, W. B. Lu and L. F. Jiao, Adv. Funct. Mater., 2024, **34**, 2400397.

7 X. Zhou, J. Li, G. Y. Zhou, W. R. Huang, Y. C. Zhang, J. Yang, H. Pang, M. Y. Zhang, D. M. Sun, Y. W. Tang and L. Xu, J. Energy Chem., 2024, **93**, 592-600.

8 L. X. Su, C. X. Cui, S. N. Zhou, H. Wu, S. K. Zhang and H. Pang, Nano Energy, 2025, **140**, 111051.

9 F. J. Shi, L. Y. Xiao, Z. L. Zhou, X. R. Zhao, Y. Liu, J. Mao, J. Y. Qin, Y. D. Deng and J. Yang, Adv. Funct. Mater., 2025, **35**, 2501070.

10 Q. Y. Liu, X. J. Mu, F. Y. Kang, S. Y. Xie, C. H. Yan and Y. Tang, Small, 2024, **20**.

11 C. F. Liu, H. Y. Bai, J. X. Feng, K. Y. An, L. Li, Z. C. Yu, L. L. Qiao, D. Liu, S. Y. Peng, H. C. Liu and H. Pan, Carbon Energy, 2025, **7**, e684.

12 X. Q. Wang, J. H. Zhou, W. G. Cui, F. Gao, Y. Gao, F. L. Qi, Y. X. Liu, X. Y. Yang, K. Wang, Z. L. Li, Y. X. Yang, J. Chen, W. P. Sun, L. X. Sun and H. G. Pan, Adv. Sci., 2024, **11**, 2401207.

13 J. Zhou, S. Qiu, X. B. Hou, T. J. Ni, C. H. Zhang, S. X. Dai, X. K. Wang, G. H. Wang, H. Q. Jiang and M. H. Huang, Angew. Chem. Int. Ed., 2025, **64**, e202503787.

14 Y. H. Wang, S. Q. Li, X. Hou, T. T. Cui, Z. C. Zhuang, Y. H. Zhao, H. Z. Wang, W. Wei, M. Xu, Q. Fu, C. X. Chen and D. S. Wang, Adv. Mater., 2024, **36**, 2412598.

15 Y. J. Zhang, W. Y. Zhang, X. W. Zhang, Y. Gao, Q. Zhao, J. P. Li and G. Liu, Small, 2024, **20**, 2405080.

16 C. T. Hsieh, C. L. Huang, Y. A. Chen and S. Y. Lu, Appl. Catal. B Environ., 2020, **267**, 118376.

17 M. Israr, S. Ali, J. Q. Zhang, Y. Zeng, M. Humayun, H. Yu, X. Chen, C. Chen and Y. D. Li, Small, 2025, **21**, 2500828.

18 F. Zhang, K. Wang, H. Zhang, S. L. Yang, M. Xu, Y. He, L. C. Lei, P. F. Xie and X. W. Zhang, Adv. Funct. Mater., 2025, **35**, 2500861.

19 T. Wang, X. Y. Liao, T. Zhang, M. L. Dai and H. Lin, Compos. Part B-Eng., 2023, **254**, 110601.

20 Y. M. Zhu, J. A. Wang, G. Weiser, M. Klingenhof, T. Koketsu, S. H. Liu, Y. C. Pi, G. Henkelman, X. Y. Shi, J. Y. Li, C. W. Pao, M. H. Yeh, W. H. Huang, P. Strasser and J. W. Ma, Adv. Energy Mater., 2025, **15**, 2500554.

21 G. C. Li, Y. L. Li, J. Dong, B. X. Sun, Z. L. Liu, J. Zheng and G. L. Li, Adv. Funct. Mater.,2025, DOI: 10.1002/adfm.202515680, e15680.

22 L. Gao, Y. Yao, Y. H. Ma, J. J. Huang, Y. Chen, L. Chen and L. S. Jia, Adv. Funct., Mater., 2025, **35**.

23 F. L. Wei, J. H. Shen, J. Y. Xie, Z. Y. Luo, L. Y. Shi, T. T. Isimjan, X. L. Yang, J. S. Qiu and B. Wu, J. Energy Chem., 2024, **98**, 472-480.

24 G. Zhang, B. Wang, J. Bi, D. Fang and S. Yang, J. Mater. Chem. A, 2019, **7**, 5769-5778.

25 T. Li, Z. Wang, L. Wang, M. Wang and Y.-Q. Liu, Appl. Catal. B Environ., 2024, **352**, 123990.

26 C. Chen, J. Long, K. Shen, X. Liu and W. Zhang, ACS Appl. Mater. Interfaces, 2022, **14**, 38677-38688.

27 Y. Ma, Y. J. Miao, G. M. Mu, D. M. Lin, C. G. Xu, W. Zeng and F. Y. Xie, Nanomaterials, 2021, **11**.

28 S. Li, H. Zhang, L. Wu, H. Zhao, L. Li, C. Sun and B. An, J. Mater. Chem. A, 2022, **10**, 9858-9868.

29 W. Y. Zhang, R. H. Guo, Q. X. Yue, Y. R. Huang, G. F. Zhang and L. L. Guan, Ionics, 2024, **30**, 3403-3416.

30 L. Li, K. Chao, X. W. Liu and S. Y. Zhou, J. Alloys Compd., 2023, **941**.

31 J. Y. Zhang, M. Y. Yang, T. Huang, J. W. Sun, W. Y. Hu, Y. Y. Li, F. Y. Yang and M. G. Ouyang, Chem. Eng. J., 2024, **493**, 152547.

32 D. Cao, J. Shao, Y. H. Cui, L. P. Zhang and D. J. Cheng, Small, 2023, **19**, 2301613.

33 A. Majumdar, K. D. Tran, S. Prabhakaran, D. Kim, D. T. Tran, N. H. Kim and J. H. Lee, Adv. Funct. Mater., 2025, **35**, 2420517.

34 Y. Shi, L. Song, Y. Liu, T. Wang, C. Li, J. Lai and L. Wang, Adv. Energy Mater., 2024, **14**, 2402046.

35 H. S. Hu, X. L. Wang, Z. R. Zhang, J. H. Liu, X. H. Yan, X. L. Wang, J. C. Wang, J. P. Attfield and M. H. Yang, Adv. Mater., 2025, **37**, 2415421.